ACS APPLIED MATERIALS & INTERFACES

Research Article

www.acsami.org

Tunable Hydrogen Separation in Porous Graphene Membrane: First-Principle and Molecular Dynamic Simulation

Yehan Tao,[†,‡] Qingzhong Xue,*[,†,‡] Zilong Liu,[‡] Meixia Shan,[‡] Cuicui Ling,[‡] Tiantian Wu,[‡] and Xiaofang Li[‡]

[†]State Key Laboratory of Heavy Oil Processing, China University of Petroleum, Qingdao 266580, Shandong, P. R. China

[‡]College of Science and Key Laboratory of New Energy Physics & Materials Science in Universities of Shandong, China University of Petroleum, Qingdao 266580, Shandong, P. R. China

Supporting Information

ABSTRACT: First-principle density functional theory (DFT) calculation and molecular dynamic (MD) simulation are employed to investigate the hydrogen purification performance of two-dimensional porous graphene material (PG-ESX). First, the pore size of PG-ES1 (3.2775 Å) is expected to show high selectivity of H_2 by DFT calculation. Then MD simulations demonstrate the hydrogen purification process of the PG-ESX membrane. The results indicate that the selectivity of H_2 over several other gas molecules that often accompany H_2 in industrial steam methane reforming or dehydrogenation of alkanes (such as N_2, CO, and CH_4) is sensitive to the pore size of the membrane. PG-ES and PG-ES1 membranes both exhibit high selectivity for H_2 over other gases, but the permeability of the PG-ES membrane is much lower than the PG-ES1 membrane because of the smaller pore size. The PG-ES2 membrane with bigger pores demonstrates low selectivity for H_2 over other gases. Energy barrier and electron density have been used to explain the difference of selectivity and permeability of PG-ESX membranes by DFT calculations. The energy barrier for gas molecules passing through the membrane generally increase with the decreasing of pore sizes or increasing of molecule kinetic diameter, due to the different electron overlap between gas and a membrane. The PG-ES1 membrane is far superior to other carbon membranes and has great potential applications in hydrogen purification, energy clean combustion, and making new concept membrane for gas separation.

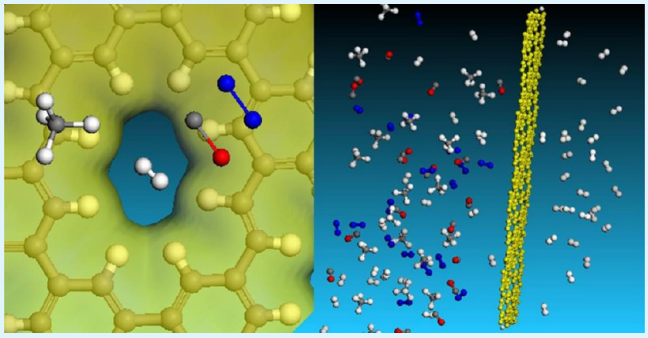

KEYWORDS: *porous graphene, hydrogen purification, density functional theory, molecular dynamics, energy barrier, size restriction*

1. INTRODUCTION

With high energy conversion efficiency, zero pollutant emission, clean-burning product, rich in energy per unit mass, and most potentially abundant source, hydrogen energy is considered as the most clean and promising alternative energy source in the future.[1−4] However, there are many less desirable byproducts associated with the manufacturing process of hydrogen (nitrogen, carbon monoxide, methane, and so on) which severely limits the further use of hydrogen. For example, carbon monoxide and methane, which are generated in the steam-reforming of methane or dehydrogenation of alkanes to produce hydrogen, cause fuel-cell catalyst poisoning when hydrogen is used as fuel-cell. Therefore, developing high-flux/high-selectivity technologies for separating mixtures of gases containing hydrogen has great importance for efficient hydrogen purification.

Membrane-based technology is gaining larger acceptance compared with other traditionally utilized separation technologies used for hydrogen purification, such as pressure swing absorption and cryogenic distillation. This is because membrane-based technology offers several benefits such as low investment cost, facile operation, large size, small footprint, and easy maintenance.[5,6] Membrane materials, such as polymer films,[7,8] zeolite,[9] carbon micropores,[10] carbon nanotubes,[11] and organic framework[12,13] have been widely used for hydrogen purification. However, these traditional membrane materials are limited in their overall selectivity/permeability for economically viable hydrogen separation, because these membrane materials have drawbacks of an inherent trade-off between selectivity and permeability.[14]

Recently, graphene, a single atomic layer carbon material with particular structural and fantastic properties, is expected as a promising membrane material for hydrogen purification. Pristine perfect graphene sheet is impermeable to gases as small as He,[15] so porous graphene (PG) is employed to achieve gas permeability.[16,17] PG is a collection of graphene-related materials with nanopores in the plane.[18,19] There are two types of PG that coexist in current publications.[20,21] One is

Received: December 20, 2013
Accepted: March 12, 2014
Published: March 12, 2014

called "top-down" PG synthesized by creating pores in the perfect graphene sheets using beam treatment, heavy ion bombardment, oxidative etching, or reducing graphene oxide mehods.[22−24] Theoretical and experimental investigations on top-down PG for hydrogen separation have been reported and provide a general understanding of the effects of pore size and chemical functionalization.[24−32] However, precise manufacture of the pores on graphene is quite challenging, and the larger pores created would decrease the selectivity of PG.[33]

The other PG is called "bottom-up" PG with precise structure morphology synthesized by a cross-coupling method, which possesses the advantage of high surface area, inherent well-defined, and large range of pore which can be densely and regularly spaced on the two-dimensional surface.[18,30] Such PG synthesized by Bieri et al.[34] has been demonstrated as efficient hydrogen,[35−37] noble gas,[38] isotope,[39] and other gas[40] separation membranes. Other bottom-up PG structures such as graphyne and graphdiyne have also been presented as excellent candidates for hydrogen purification.[41−43] In the view of industrial applications, a series of bottom-up PG has been successfully synthesized. Bieri et al. used a Ag surface-promoted aryl−aryl coupling reaction to produce a covalently linked hydrocarbon superhoneycomb network.[34] Large-area graphdiyne has been made by Li et al. using Cu-surface promoted cross-coupling reaction from hexaethynylbenzene.[44] Other similar porous structures, such as porous polyphenylene frameworks,[45] two-dimensional dimethyl-methylene-bridged triphenylamine,[46] two-dimensional 1,4-benzenediboronic acid,[47] two-dimensional polyester,[48] and borazine polymer,[49] have also been successfully obtained. These all demonstrate the growing ability to synthesize bottom-up PG such as the one we used in our investigation.

The PG we used here is designed by Schrier et al., which is analogous to the periodic PG structure synthesized by Bieri et al., but extended in one direction by E-stilbene-like units. Depending on the number (X) of the adding E-stilbene-like units (ES), the membrane yields structures denoted as PG-ESX.[38,50] When adding no E-stilbene-like unit (X = 0), the PG-ES membrane is the PG structure synthesized by Bieri et al. (which is called a two-dimensional polyphenylene (2D-PP) in their work). In this paper, first-principle density functional theory (DFT) calculation and molecular dynamic (MD) simulation are used to study the performance of PG-ESX membranes on hydrogen purification. We investigate the effect of pore size of PG-ESX membranes for hydrogen purification by DFT calculation. Then MD simulation shows the dynamic hydrogen separation process. Finally, the energy barrier and the electron density are employed to explain the separation mechanism. Theoretical computations have been conducted to open up exciting opportunities for construction of molecular sieve membranes to meet different hydrogen separation needs.

2. MODELS AND METHODS

DFT calculations show the mechanism of hydrogen purification using PG-ESX membranes. Spin-unrestricted all-electron DFT calculations employed the generalized gradient approximation (GGA) based on Perdew-Burke-Ernzerhof (PBE), which interprets the nonhomogeneity of the true electron density using the gradient of charge density, for exchange-correlation functional.[26,38] The double numerical basis set augmented with polarization p-function (DNP) was used for the expanded electronic wave function. All the atomic coordinates were optimized by 10^{-6} a.u. SCF tolerance, 10^{-5} a.u. energy, 0.002 au/Å force, and 0.005 Å maximum displacement convergence criteria. A real-space global orbital cutoff radius of 6.0 Å and a smearing point of 0.002 Ha were used. The Brillouin zone was represented by Monkhorst-Pack special k-points of 6 × 6 × 1 meshes. A vacuum thickness of 20 Å was employed along the z direction of the PG-ESX sheets. These simulation parameters were generally applied in our previous works.[51,52] In addition, since atom-centered basis functions were employed for DFT calculations, the counterpoise correction for the presence of basis set superposition errors (BSSE) was included in the calculation. Dispersion correction for DFT calculation (DFT-D) had also been considered by using Grimme's method.[53]

MD simulations show the hydrogen purification process. The interatomic interactions in MD were described by the force field of a condensed-phase optimized molecular potential for atomistic simulation studies (COMPASS).[54] COMPASS is a first *ab initio* force field, and most parameters are derived by *ab initio* parametrization and empirical optimization. COMPASS force field has been proven to enable accurate and simultaneous prediction of structural, conformational, vibrational, cohesive, thermophysical, and various gas-phase properties for a broad range of compounds, both in isolation and in condensed phases.[55,56] The Anderson thermostat method was employed to control the temperature of the system. The vdW interactions were calculated within a cutoff distance of 9.5 Å, and the Ewald method was applied for the calculation of electrostatic interactions. Interactions between gas molecules, and between gas molecules and PG-ESX membranes, were treated using a Lennard-Jones potential.[38] These simulation parameters were also generally applied in our previous works.[57,58] The gas mixture involved 54 H_2 and 54 other gas molecules. Two PG-ESX membranes were used in both sides of the gas mixture to enhance the gas permeability and minimize the influence of the fixed wall. Then vacuum space was built besides two sides of the gas mixture and was defined as the side box. We then put the model into an NVT ensemble, a fixed time step of 1 fs was used, and data was collected every 5 ps. The full-precision trajectory was then recorded, and the results were analyzed. According to the literature, hydrogen atoms of the PG-ESX membranes surrounding the penetrated pores were fully relaxed, while carbon atom coordinates perpendicular to the membrane plane were kept fixed.[33] Periodic boundary conditions were applied in all three dimensions in both DFT and MD simulations. Our DFT calculation and MD simulation were carried out using DMol^3 and Discover codes embedded in the Material Studio software, respectively.

3. RESULTS AND DISCUSSION

3.1. Pore Size of PG-ESX. H_2 demonstrates a significant difference in its molecular kinetic diameter compared with other gases (2.9 Å for H_2, 3.64 Å for N_2, 3.76 Å for CO, and 3.8 Å for CH_4), because H_2 has only two electrons on a fairly compact 1s orbital and hence possesses smaller kinetic diameter. H_2 is expected to be separated from other gas molecules by a candidate pore size of the separation membrane that can block other gas molecules with a bigger kinetic diameter than H_2. The key factor in utilizing the size restriction for hydrogen separation is designing membranes with appropriate pore width that has the optimal balance between selectivity and permeability. In this paper, PG-ESX membranes with different pore size are employed to look for the most appropriate hydrogen separation membrane.

First, for further confirming the stability of PG-ESX membranes, we performed a high-quality DFT geometry optimization to PG-ESX membranes, and the unit cell was fully relaxed during this process. The DFT calculation we employed here is highly accurate, thus the associated computational workload is very high. In order to save calculation time, we only compute dozens of atoms in the simulation. DFT calculation is carried out using a 2 × 2 PG-ESX supercell to simulate infinite planar sheets. From the result, PG-ESX membranes provide to be nearly flat two-dimensional membranes without significant deformation. The

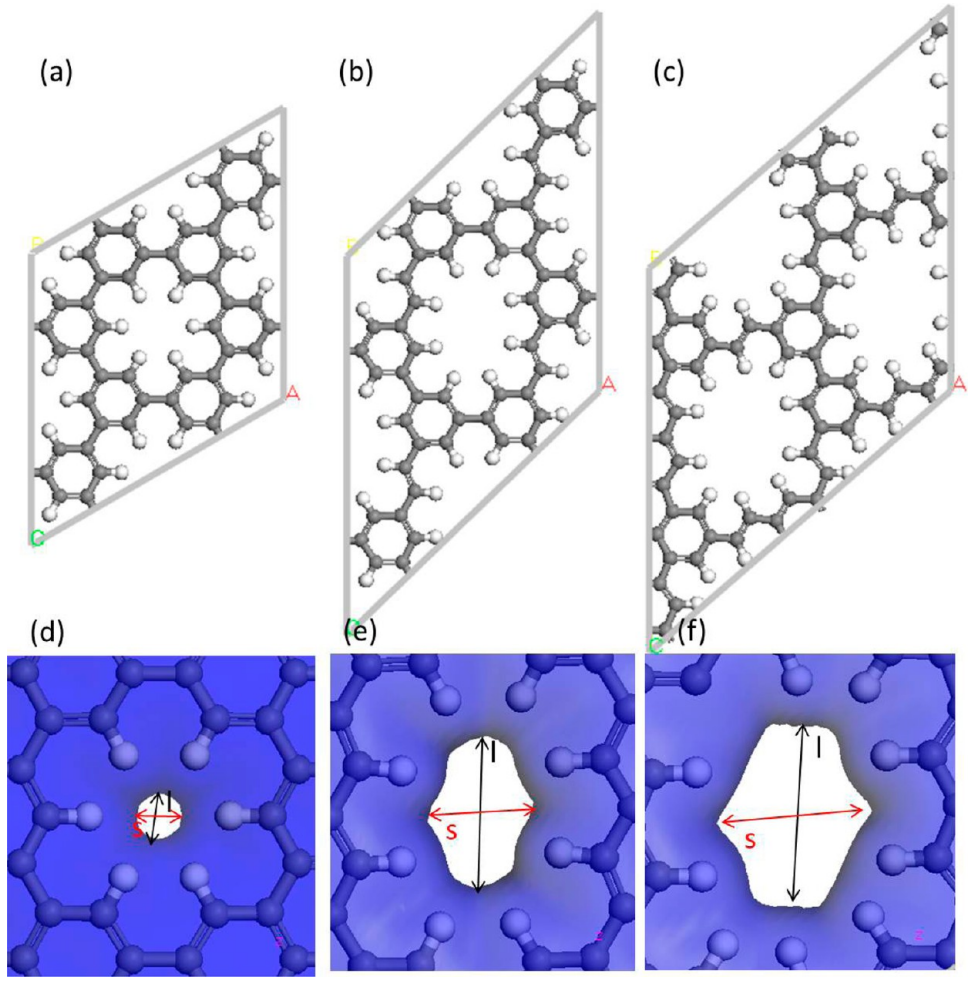

Figure 1. Structure of (a) PG-ES, (b) PG-ES1, and (c) PG-ES2. Pore electron denstity isosurface of (d) PG-ES, (e) PG-ES1, and (f) PG-ES2 (isovalue of 0.02 e/Å^3).

optimized lattice parameters are $a = b = 7.439$ Å for the PG-ES supercell, $a = 9.237$ Å, $b = 9.9569$ Å for the PG-ES1 supercell, and $a = 10.247$ Å, $b = 9.845$ Å for the PG-ES2 supercell. These structure parameters of optimized PG-ESX structures match well with previous theoretical and experimental studies,[38,59] for example, the optimized lattice parameters for PG-ES are $a = b = 7.455$ Å in theory[36] and $a = b = 7.4$ Å in experiment.[34] Figure 1(a)−(c) shows the structures of PG-ES, PG-ES1, and PG-ES2. More information about coordinate parameters of PG-ESX structures are listed in the Supporting Information.

Then we investigate the pore size of PG-ESX membranes. Figure 1(d)−(f) shows the electron density isosurface of the 2 × 2 PG-ESX supercell at an isosurface value of 0.02 e/Å^3. The pore of PG-ES is hexagonal in shape, while the pores of PG-ES1 and PG-ES2 could be seen to be approximately rectangular in shape. Pore size is characterized as the average of the short side (s) and long side (l) in the hexagonal or rectangular region within the pores. The pore area is estimated according to the area of the hexagonal or rectangular region (product of s and l). The corresponding pore parameters are shown in Table 1. The pore size of PG-ES (1.3545 Å) is much smaller than all the kinetic diameters of gases, and the pore size of PG-ES2 (3.8165 Å) is bigger than all the kinetic diameters of gases. However, the pore size of PG-ES1 (3.2775 Å) is slightly bigger than the kinetic diameter of H_2 but much smaller than that of N_2, CO, and CH_4, which might be suitable for efficient H_2 separation.

Table 1. Pore Parameters of the PG-ESX Membrane

	PG-ES	PG-ES1	PG-ES2
s/Å[a]	1.341	2.531	3.221
l/Å[a]	1.368	4.024	4.412
pore size/Å	1.3545	3.2775	3.8165
pore area/Å^2	1.834488	10.18474	14.21105

[a] s and l represent for short side and long side in the hexagonal or rectangular region within the pores.

The result of the pore size of PG-ES1 is in good agreements with the previous studies with the same isosurface value.[26]

3.2. MD Simulation for Hydrogen Purification. On the basis of pore size of PG-ESX membranes by DFT calculation, MD simulation with more atom numbers was performed to observe the hydrogen purification by PG-ESX membranes. Nine simulation models with different membranes or different gas mixtures were simulated. Because of the difference in the lattice parameter of PG-ESX membranes, the models we constructed with different PG-ESX membranes have a small difference in dimensions. The detailed dimensions of simulation models are available in the Supporting Information. We employ the example of using the PG-ES1 membrane to separate the H_2/N_2 mixture to show the separation process (see Figure 2). The snapshots of the H_2/N_2, H_2/CO, and H_2/CH_4 mixtures penetrating through PG-ESX membranes in the

dx.doi.org/10.1021/am4058887 | ACS Appl. Mater. Interfaces 2014, 6, 8048−8058

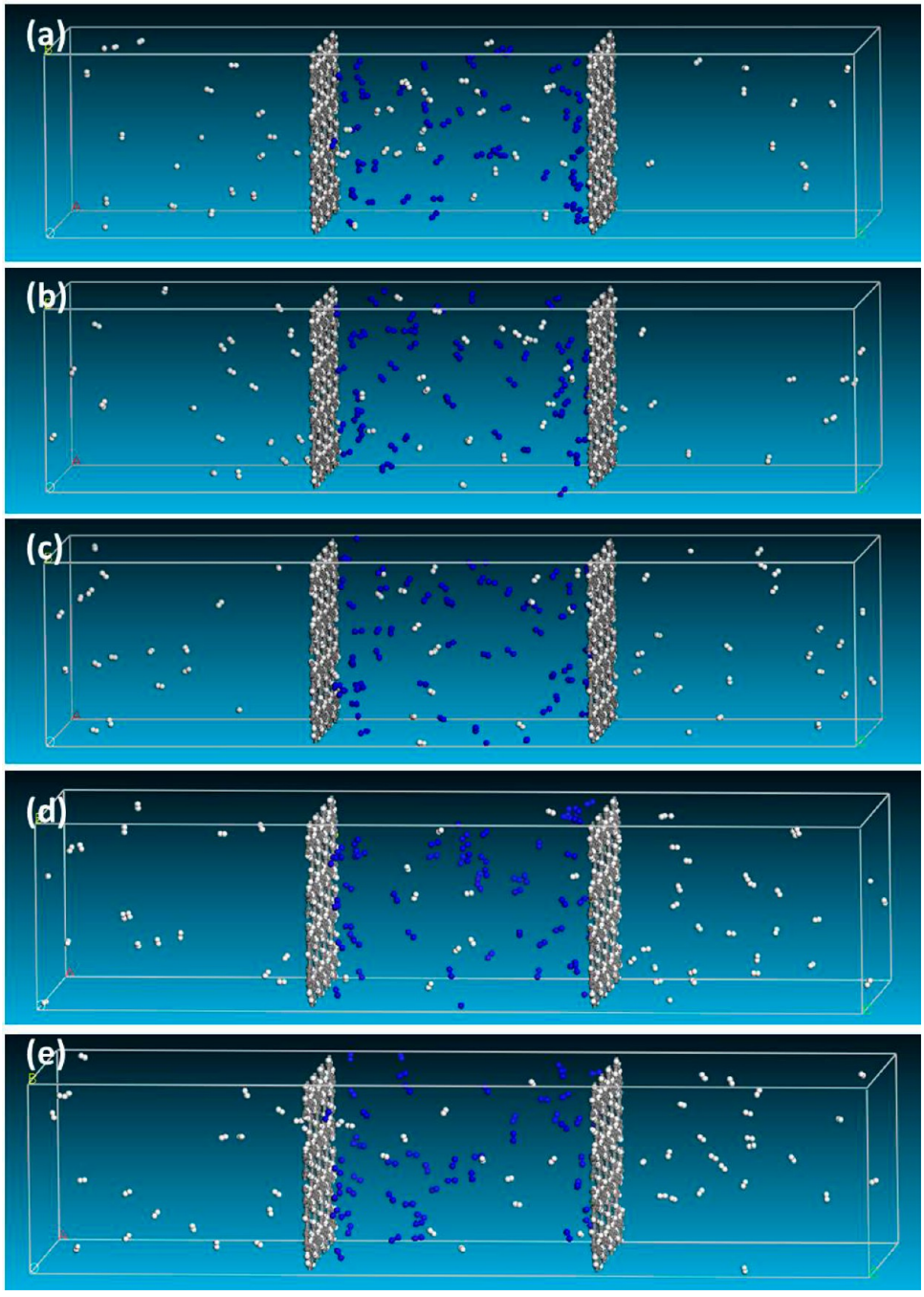

Figure 2. Snapshots of configuration of the H_2/N_2 mixture permeating through the PG-ES1 membrane at (a) 0.3 ns, (b) 0.5 ns, (c) 1 ns, (d) 3 ns, and (e) 5 ns. Hydrogen, carbon, and nitrogen atoms are colored by white, gray, and blue, respectively. The membrane model was constructed with dimensions of 36.94 Å × 28.64 Å × 126.3 Å.

simulation from 0 to 5 ns can be found in Figures S1−S8 in the Supporting Information.

In most cases, the permeation process can be divided into three steps. First, gas molecules approach to the membrane pore. Then, they linger on the surface near the pore for a few picoseconds before successfully crossing the barrier. Finally, it goes to the other side of the membrane. We counted the permeation events of two membranes, and we just considered molecules crossed to the side boxes at the end of the simulation. In the H_2/N_2 separation process of the PG-ES1 membrane, one H_2 molecule goes through the pore of the PG-ES1 membrane at t = 5 ps. It can be seen in Figure 2 that as the number of simulation time steps increased, more H_2 molecules diffuse through the membrane to the side boxes. At t = 5 ns, 40 H_2 molecules cross the pore, while there is no N_2 molecule observed to penetrate through the PG-ES1 membrane during a 5 ns simulation. We also tested extended simulation time (20 ns) for each kind of PG-ESX membrane and found that all the systems reached a balanced state in 3−4 ns. We consider that a 5 ns simulation time is long enough for our system to obtain some regular results. We compare our results with that presented in ref 50. Schrier demonstrated that PG-ES1 is slightly permeable to N_2 (two N_2 passed the PG-ES1 membrane) at high-pressure, and there is no N_2 passing

dx.doi.org/10.1021/am4058887 | ACS Appl. Mater. Interfaces 2014, 6, 8048−8058

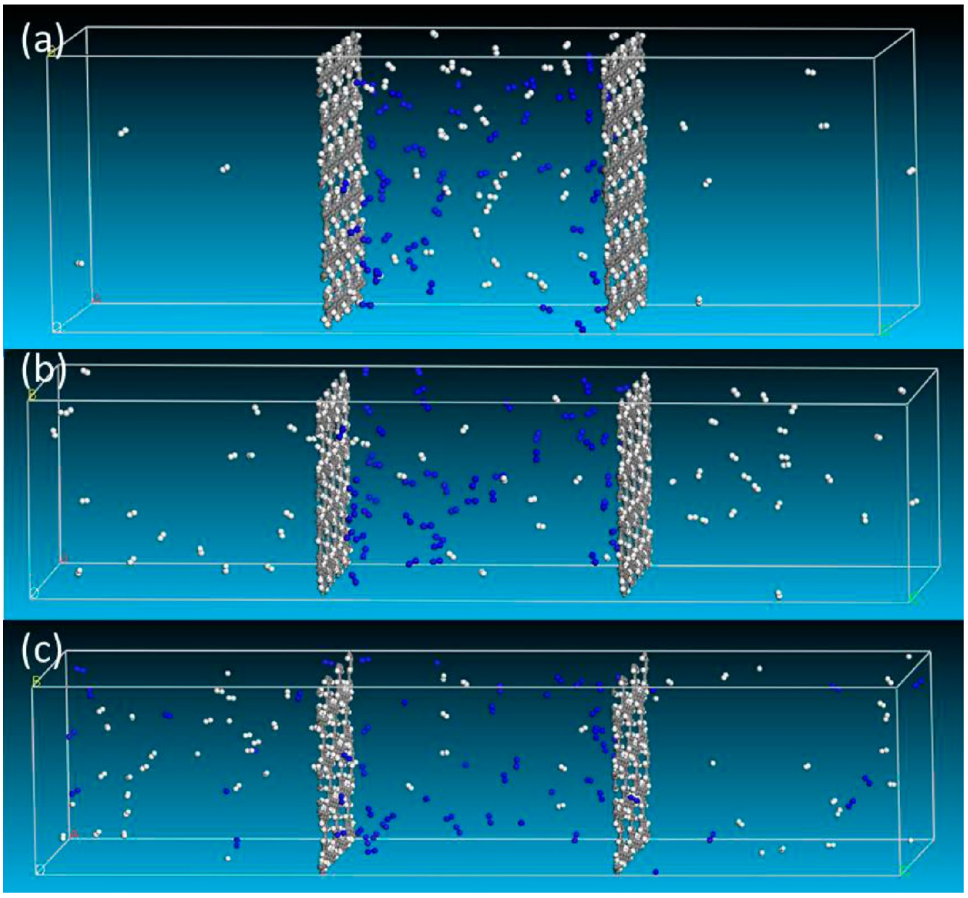

Figure 3. Final configuration of the H_2/N_2 mixture permeating through (a) PG-ES, (b) PG-ES1, and (c) PG-ES2 membranes. Hydrogen, carbon, and nitrogen atoms are colored by white, gray, and blue, respectively.

through the PG-ES1 membrane at medium- and low-pressure. This small difference between their results and ours come from two reasons. First, the temperature they used (325 K) is higher than ours (298 K), and we know that temperature is a key factor in the gas separation process. Second, the high pressure they employed also has a benefit for N_2 passing through the pore. As far as we are concerned, it is hard for N_2 molecules to penetrate through the pore of PG-ES1 even at high temperature or high feed pressure.

Figures 3, 4 and 5 show the final configurations of H_2/N_2, H_2/CO, and H_2/CH_4 mixtures permeating through the PG-ESX membranes after a 5 ns simulation process under 298 K, respectively. When we used the PG-ES or the PG-ES1 membrane for gas separation, only H_2 molecules can penetrate through the membrane. However, only a few (less than 10) H_2 molecules passed through the PG-ES membrane during a 5 ns simulation process, compared to 30−40 H_2 molecules passing through the PG-ES1 membrane during the same 5 ns simulation process. This is because the pore size of PG-ES (1.3545 Å) is too small for all four gas molecules and make it hard for gas molecules to pass through the pore, while the pore size of PG-ES1 (3.2775 Å) is slightly bigger than the kinetic diameter of H_2 (2.9 Å), which is suitable for H_2 penetration. When we used the PG-ES2 membrane with a pore size of 3.8165 Å, all four gas molecules can penetrate through the pore, because the pore size is bigger than the kinetic diameter of all four gas molecules. The MD results match well with DFT predictions by calculating the pore size. As a result, PG-ES and PG-ES1 membranes show excellent selectivity of H_2 over N_2, CO, and CH_4. In the case of the PG-ES2 membrane, we use the definition of selectivity as we previously used to demonstrate the selectivity of the PG-ES2 membrane.[57] The selectivity of A over B is defined as follows[43]

$$S_{A/B} = \frac{x_A/y_A}{x_B/y_B} \tag{1}$$

where x and y are the mole fractions of the components in the side boxes and gas mixture. While the initial H_2/other gas ratio is 1, the selectivity of H_2 over other gas can be simply defined as the ratio of H_2/other gas in the side boxes at the end of the simulation. The selectivity of H_2/N_2, H_2/CO, and H_2/CH_4 for the PG-ES2 membrane is 2.81, 2.6. and 8.75, respectively. The selectivity of the PG-ES2 membrane is really low, making it unsuitable for hydrogen purification.

We use the molecular flow to further characterize the permeability of PG-ESX membranes quantitatively, which is defined as[27]

$$F = \frac{N(mol)}{S(m^2)T(s)} \tag{2}$$

where N is the mole of the gas molecules that permeate through the membrane, S refers to the area of the membrane in total, and T is the simulation time. We compute the flow of gas at the end of the simulation. Figure 6 shows the number of gas observed crossings and molecular flow for PG-ESX membranes during a 5 ns simulation as a function of the pore area. It is obvious that the number of gas passing through the pore and

dx.doi.org/10.1021/am4058887 | ACS Appl. Mater. Interfaces 2014, 6, 8048−8058

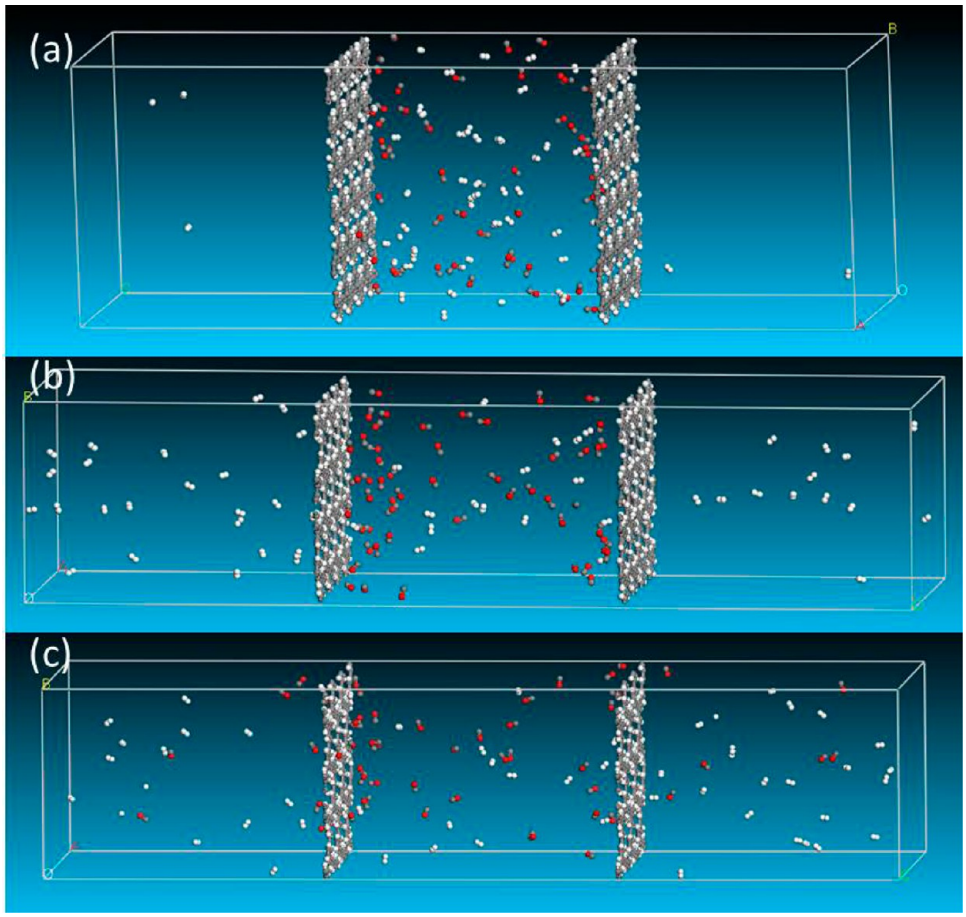

Figure 4. Final configuration of the H_2/CO mixture permeating through (a) PG-ES, (b) PG-ES1, and (c) PG-ES2 membranes. Hydrogen, carbon, and oxygen atoms are colored by white, gray, and red, respectively.

molecular flow sensitively increase with the pore size, which is in accord with the previous study.[27] The permeability of the PG-ES membrane is not satisfied, making it improper for hydrogen purification. As for the PG-ES1 membrane, about 75% H_2 molecules (35−40 gas molecules) in the feed gas mixture can pass through the PG-ES1 membrane and demonstrates an average H_2 flow of 1300 mol/m^2·s. Both the advantage of high surface area and well-defined large range of pore make contributions to the high selectivity and permeability of the PG-ES1 membrane.

Compared to the previous report of hydrogen purification of other carbon membranes, our simulation results suggest that the PG-ES1 membrane can only allow H_2 molecules to pass through, which means the selectivity of PG-ES1 is much higher than the selectivity of H_2/N_2 of top-down PG (with a selectivity of 9)[27] and the selectivity of H_2/CH_4 of the carbon nanotube (with selectivity in the range of 15−51).[60] The H_2 permeability of the PG-ES1 membrane is also higher than the carbon nanotube for hydrogen purification,[11] which means the PG-ES1 membrane is far superior to other porous carbon membranes. The PG-ES1 membrane with a single atom thickness has overcome an inherent trade-off of traditional membrane materials between selectivity and permeability and is expected to have great potential applications in industrial hydrogen purification applications.

3.3. Energy Barrier for Gas Molecules Crossing PG-ESX Membranes. In order to further explain the mechanism of the different capabilities of PG-ESX membranes for separating H_2 from other gases, interaction energy (E_{int}) and electron density between different gas molecules and PG-ESX membranes are computed by DFT calculations. Apparently, the configurations of the gas in the middle of the pore have a significant effect on E_{int}.[26,33,36,41] We first examined several configurations for H_2, N_2, CO, and CH_4 placed in the middle of the pore of PG-ESX membranes to figure out the most energetically stable configurations for the gas molecules to penetrate through the membrane. The detailed selection process can be found in Figures S9−S12 in the Supporting Information. The corresponding E_{int} have been listed in Tables S1−S4 in the Supporting Information. Seen from the results, for linear H_2, N_2, and CO molecules, the most energetically stable configurations are shown to be the axis of the molecules perpendicular to the surface of the membranes, while for tetrahedral CH_4 molecules, it is the four H atoms of CH_4 pointing toward the four corners of the hexagonal or rectangular pore. It can be intuitively speculated that these energetically stable orientations in the middle of the pore are favored for gas molecules to minimize the energy barrier during the penetration process, so we choose these configurations for the following E_{int} calculations.

We specified a total of 31 points along Z axis of the PG-ESX membranes which is perpendicular to the plane of PG-ESX membranes and passing the center of the pore. The distance from the center of mass of the gas molecules to the center of the pore is plotted as the X axis in Figure 7 which also means the adsorption height. The spacing between points is 0.2 Å. E_{int}

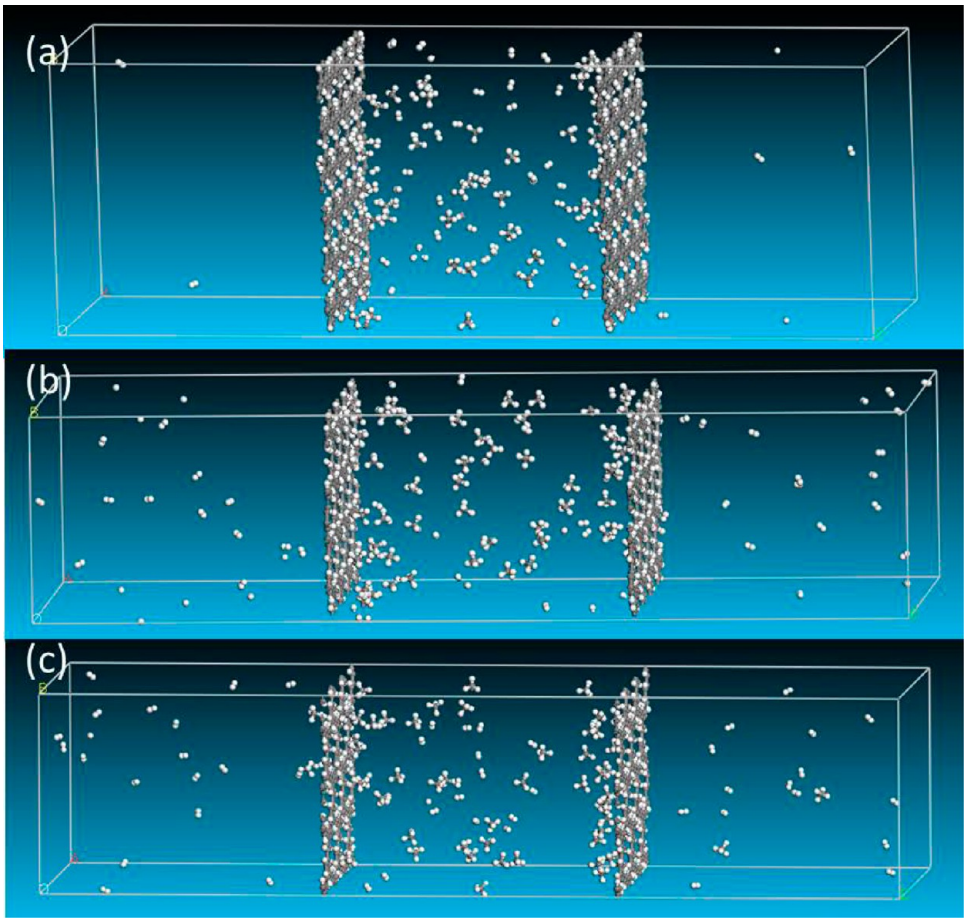

Figure 5. Final configuration of the H_2/CH_4 mixture permeating through (a) PG-ES, (b) PG-ES1, and (c) PG-ES2 membranes. Hydrogen and carbon atoms are colored by white and gray, respectively.

is obtained by progressively varying the adsorption height, and the gas molecules are fixed at each of these points. E_{int} is calculated by the following equation

$$E_{int} = E_{PG\text{-}ESX+gas} - (E_{PG\text{-}ESX} + E_{gas}) \quad (3)$$

where $E_{PG\text{-}ESX+gas}$ is the total energy of the PG-ESX membranes and gas molecules, $E_{PG\text{-}ESX}$ is the energy of pure PG-ESX membranes, and E_{gas} is the energy of isolated gas molecules. Figure 7 shows E_{int} between gas molecules and the PG-ESX membranes as a function of adsorption height. The maximum value in the curve of E_{int} is defined as the energy barrier for gas molecules penetrating through the membrane. The energy barriers are listed in Table 2.

The energy barrier appears at different adsorption height for nonpolar and polar gases in PG-ES pores. For polar molecule CO, when the O atom is in the middle of the pore, the system shows the maximum E_{int}. This is because the O atom of CO molecule with electronegativity interacted strongly with H atoms at the edge of the pore of the PG-ES membrane which have electropositivity. For nonpolar molecules H_2, N_2, and CH_4, the systems show the maximum E_{int} when the center of mass of the molecules are in the middle of the pore of PG-ES1. However, when the PG-ES1 and PG-ES2 membranes with bigger pore size are used for computing E_{int}, all four gases show the maximum E_{int} when the center of mass of the molecules is in the middle of the pore which means the effect of gas polarity can be ignored.

It can be clearly seen in Figure 7 that the energy barriers sensitively depend on the pore size of membranes and molecular kinetic diameters. Small pore size and big molecular kinetic diameters both cause a higher repulsive interaction that creates a high energy barrier for gas molecules to pass through the pore. The H_2 molecule exhibits a much lower energy barrier when penetrating through the PG-ES (0.63 eV) or the PG-ES1 (0.12 eV) membrane compared to N_2, CO, and CH_4 molecules. H_2 molecules can get separated by the PG-ES (with an energy barrier of 2.19 eV for N_2, 2.86 eV for CO, and 4.51 eV for CH_4) or the PG-ES1 (with an energy barrier of 0.26 eV for N_2, 0.25 eV for CO, and 0.82 eV for CH_4) membrane, because larger molecules are completely blocked by the relatively higher energy barrier. In the case of the PG-ES2 membrane, the energy barrier for all four molecules penetrating through the PG-ES2 membrane decreases drastically (−0.02 eV for H_2, −0.1 eV for N_2, 0.02 eV for CO, and 0.21 eV for CH_4). The E_{int} curves for H_2, N_2, and CO are nearly constant for molecules moving in and out of the pore, which means the restriction of the pore size to the molecules permeation vanishes. The energy barrier for the H_2 or the N_2 passing PG-ES2 membrane is negative, which means the pore shows an attractive E_{int} when the gas molecule is in the middle of the pore. This is because that the distance between the atom at the edge of the pore of PG-ES2 and gas molecules is big enough that E_{int} reaches to the range of attractive interaction. Although the pore of PG-ES2 still shows a small repulsive E_{int} for CO and CH_4 molecules, this moderate energy barrier can be easily overcome by CO or CH_4

dx.doi.org/10.1021/am4058887 | ACS Appl. Mater. Interfaces 2014, 6, 8048−8058

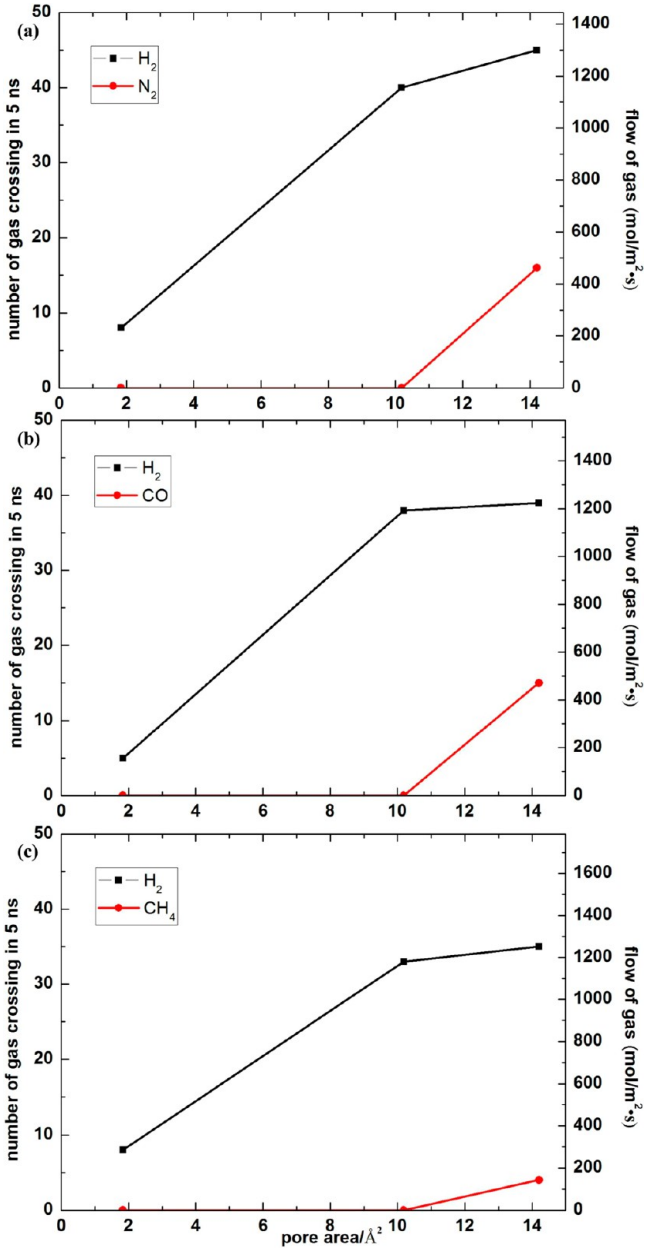

Figure 6. Crossing molecule number and flow of (a) H_2/N_2, (b) H_2/CO, and (c) H_2/CH_4 mixtures as a function of the pore area.

molecules under experimental conditions. We compared our DFT results of energy barrier with other published works, for example, the energy barrier for H_2, CO, and CH_4 penetrating through PG-ES is 0.61 eV, 2.35 eV, and 5.19 eV in ref 36, respectively, while the energy barrier for H_2 and CO penetrating through PG-ES is 0.37 eV and 1.7 eV in ref 35, respectively. It is found that our result is acceptable with little difference caused by different computational methodologies.

In addition, as the interactions between gas molecules and membranes are weak interactions, it is crucial to consider dispersion corrections in the DFT calculations. After calculation E_{int} with DFT-D, we find that the difference between E_{int} with or without DFT-D is very small (less than 0.01 eV) and is not going to change the qualitative results we have gotten previously. This difference is so small that we even cannot distinguish it when we put the curves of E_{int} with or without DFT-D together. The corresponding E_{int} with or without DFT-D is shown in the Supporting Information.

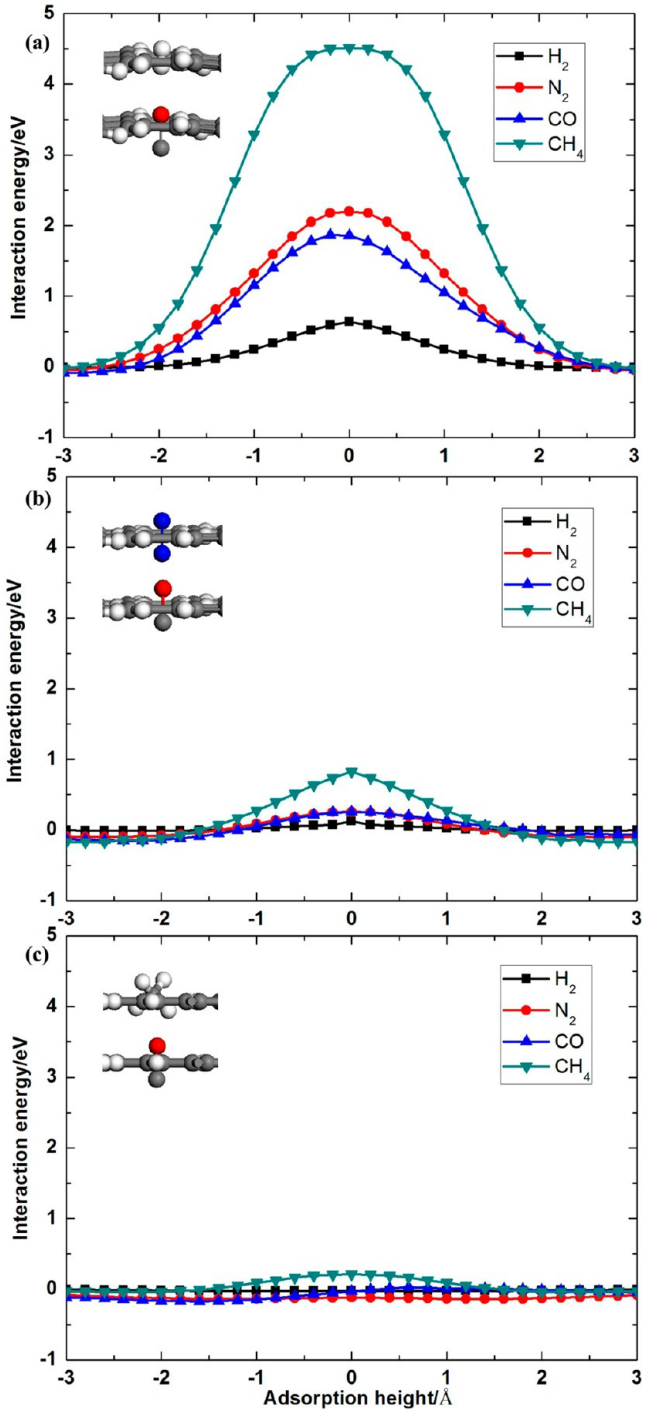

Figure 7. Interaction energy between gas molecules and (a) PG-ES, (b) PG-ES1, and (c) PG-ES2 membranes as a function of adsorption height.

Table 2. Energy Barrier of H_2, N_2, CO, and CH_4 for Passing PG-ESX Membranes/eV

	PG-ES	PG-ES1	PG-ES2
H_2	0.637	0.127	−0.022
N_2	2.199	0.258	−0.118
CO	1.863	0.256	0.028
CH_4	4.517	0.826	0.213

dx.doi.org/10.1021/am4058887 | ACS Appl. Mater. Interfaces 2014, 6, 8048−8058

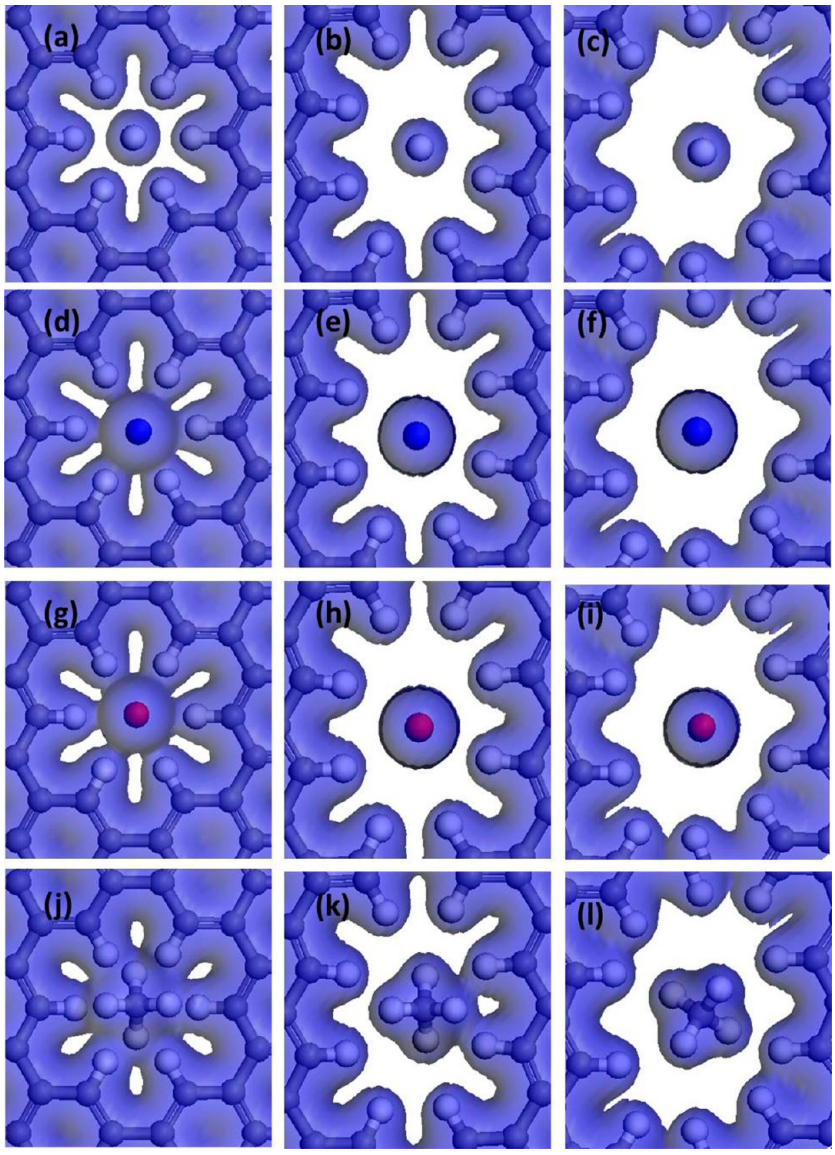

Figure 8. Electron-density isosurface for (a)−(c) H_2, (d)−(f) N_2, (g)−(i) CO, and (j)−(l) CH_4 passing through the pores of PG-ES, PG-ES1, and PG-ES2 membranes, respectively (isovalue of 0.15 e/Å^3).

3.4. Electron Density of Gas Molecules Interact with PG-ESX Membranes. For a deeper understanding of the energy barrier difference, we plot the electron density isosurfaces for the four molecules interacting with PG-ESX membranes (see in Figure 8). For all three kinds of PG-ESX membranes, the electron overlap between H_2 and the pore of PG-ESX is less pronounced than those of N_2, CO, and CH_4. Obviously, CH_4 has the most pronounced electron overlap with PG-ESX membranes, resulting in the highest energy barrier. This is because that as the kinetic diameter of the molecule becomes larger, the distance between the molecule and the pore becomes narrower, invoking charge closing between molecules and adjacent hydrogen atoms of PG-ESX membranes. For the same gas molecule, the electron overlap between the molecule and the pore of PG-ES2 is much smaller than that of PG-ES or PG-ES1, leading to a much lower energy barrier for molecules penetrating through the PG-ES2 membrane. Therefore, intrinsically it is the electron densities at the pores that hinders the molecules to pass through the pores. The results of the electron density of the system are in good agreement with the previous studies with same isosurface value.[36] Generally speaking, H_2 can pass though the pore of PG-ESX with a smaller energy barrier and less pronounced electron overlap. However, the diffusion of N_2, CO, and CH_4 molecules is more difficult.

4. CONCLUSIONS

In summary, the hydrogen purification performance of the PG-ESX membrane has been investigated via DFT and MD computations. Considering that the pore of PG-ES (1.3545 Å) appears to be too small, whereas that of PG-ES2 (3.8165 Å) is relatively large for separating H_2 from other gases, PG-ES1 membrane material with appropriate pore size of 3.2775 Å is expected as an excellent candidate for hydrogen purification. MD simulation shows that about 75% H_2 in the feed gas mixture can pass through the PG-ES1 membrane and demonstrates an average H_2 flow of 1300 mol/m^2·s. DFT calculations successfully explain the MD simulation results by calculating energy barrier and electron density. The energy barrier for H_2, N_2, CO, and CH_4 molecules penetrating through

the PG-ES1 membrane is 0.12 eV, 0.26 eV, 0.25 eV, and 0.82 eV, respectively. Intrinsically, it is the electron overlap between the gas molecules and the pore that causes the energy barrier and hinders the molecules to pass through the pores. The PG-ES1 membrane is far superior to other carbon membranes and had great potential applications in hydrogen purification, energy clean combustion, and new concept membrane for gas separation. Such a great membrane material might be arranged in conditional gas separation membranes that would allow fast and efficient separation of different molecular species (such as hydrogen/organic gases and some organic gas mixtures including benzene/cyclohexane and propylene/propane) and can revolutionize the gas separation industry.

■ ASSOCIATED CONTENT

Supporting Information

Cell vectors and coordinates of PG-ESX unit cells for DFT calculation, snapshots of configuration of gas mixtures permeating PG-ESX membranes, the selection process of configurations for gas molecules passing through PG-ESX membranes, and the comparison between E_{int} with or without DFT-D. This material is available free of charge via the Internet at http://pubs.acs.org.

■ AUTHOR INFORMATION

Corresponding Author

*Phone: +86-0532-86981169. Fax: +86-0532-86981169. E-mail: xueqingzhong@tsinghua.org.cn.

Notes

The authors declare no competing financial interest.

■ ACKNOWLEDGMENTS

This work is supported by the Natural Science Foundation of China (11374372, 41330313), Taishan Scholar Foundation (ts20130929), the Fundamental Research Funds for the Central Universities (13CX05004A, 13CX05009A), and National Super Computing Center in Jinan.

■ REFERENCES

(1) Jain, I. Hydrogen the Fuel for 21st Century. *Int. J. Hydrogen Energy* **2009**, *34*, 7368−7378.
(2) Dunn, S. Hydrogen Futures: Toward a Sustainable Energy System. *Int. J. Hydrogen Energy* **2002**, *27*, 235−264.
(3) Momirlan, M.; Veziroglu, T. N. The Properties of Hydrogen as Fuel Tomorrow in Sustainable Energy System for a Cleaner Planet. *Int. J. Hydrogen Energy* **2005**, *30*, 795−802.
(4) Andrews, J.; Shabani, B. Re-envisioning the Role of Hhydrogen in a Sustainable Energy Economy. *Int. J. Hydrogen Energy* **2012**, *37*, 1184−1203.
(5) Bernardo, P.; Drioli, E.; Golemme, G. Membrane Gas Separation: A Review/State of the Art. *Ind. Eng. Chem. Res.* **2009**, *48*, 4638−4663.
(6) Jiao, Y.; Du, A.; Hankel, M.; Smith, S. C. Modelling Carbon Membranes for Gas and Isotope Separation. *Phys. Chem. Chem. Phys.* **2013**, *15*, 4832−4843.
(7) Low, B. T.; Xiao, Y.; Chung, T. S.; Liu, Y. Simultaneous Occurrence of Chemical Grafting, Cross-linking, and Etching on the Surface of Polyimide Membranes and Their Impact on H_2/CO_2 Separation. *Macromolecules* **2008**, *41*, 1297−1309.
(8) Chung, T. S.; Shao, L.; Tin, P. S. Surface Modification of Polyimide Membranes by Diamines for H_2 and CO_2 Separation. *Macromol. Rapid Commun.* **2006**, *27*, 998−1003.
(9) Yilmaz, G.; Keskin, S. Predicting the Performance of Zeolite Imidazolate Framework/Polymer Mixed Matrix Membranes for CO_2, CH_4, and H_2 Separations Using Molecular Simulations. *Ind. Eng. Chem. Res.* **2012**, *51*, 14218−14228.
(10) Kumar, K. V.; Müller, E. A.; Rodríguez-Reinoso, F. Effect of Pore Morphology on the Adsorption of Methane/hydrogen Mixtures on Carbon Micropores. *J. Phys. Chem. C* **2012**, *116*, 11820−11829.
(11) Bucior, B. J.; Chen, D.-L.; Liu, J.; Johnson, J. K. Porous Carbon Nanotube Membranes for Separation of H_2/CH_4 and CO_2/CH_4 Mixtures. *J. Phys. Chem. C* **2012**, *116*, 25904−25910.
(12) Herm, Z. R.; Swisher, J. A.; Smit, B.; Krishna, R.; Long, J. R. Metal - Organic Frameworks as Adsorbents for Hydrogen Purification and Precombustion Carbon Dioxide Capture. *J. Am. Chem. Soc.* **2011**, *133*, 5664−5667.
(13) Yang, Z.; Cao, D. Effect of Li Doping on Diffusion and Separation of Hydrogen and Methane in Covalent Organic Frameworks. *J. Phys. Chem. C* **2012**, *116*, 12591−12598.
(14) Robeson, L. M. The Upper Bound Revisited. *J. Membr. Sci.* **2008**, *320*, 390−400.
(15) Bunch, J. S.; Verbridge, S. S.; Alden, J. S.; van der Zande, A. M.; Parpia, J. M.; Craighead, H. G.; McEuen, P. L. Impermeable Atomic Membranes from Graphene Sheets. *Nano Lett.* **2008**, *8*, 2458−2462.
(16) Hauser, A. W.; Schrier, J.; Schwerdtfeger, P. Helium Tunneling Through Nitrogen-functionalized Graphene Pores: Pressure- and Temperature-Driven Approaches to Isotope Separation. *J. Phys. Chem. C* **2012**, *116*, 10819−10827.
(17) Hauser, A. W.; Schwerdtfeger, P. Nanoporous Graphene Membranes for Efficient $^3He/^4He$ Separation. *J. Phys. Chem. Lett.* **2012**, *3*, 209−213.
(18) Xu, P.; Yang, J.; Wang, K.; Zhou, Z.; Shen, P. Porous Graphene: Properties, Preparation, and Potential Applications. *Chin. Sci. Bull.* **2012**, *57*, 2948−2955.
(19) Kim, W.-g.; Nair, S. Membranes From Nanoporous 1D and 2D Materials: A Review of Opportunities, Developments, and Challenges Chemical Engineering. *Science* **2013**, *104*, 908−924.
(20) Russo, P.; Hu, A.; Compagnini, G. Synthesis, Properties and Potential Applications of Porous Graphene: A Review. *Nano-Micro Lett.* **2013**, *5*, 260−273.
(21) Jiang, L.; Fan, Z. Design of Advanced Porous Graphene Materials: from Graphene Nanomesh to 3D Architectures. *Nanoscale* **2014**, *6*, 1922−1945.
(22) Fischbein, M. D.; Drndic, M. Electron Beam Nanosculpting of Suspended Graphene Sheets. *Appl. Phys. Lett.* **2008**, *93*, 113107.
(23) Lehtinen, O.; Kotakoski, J.; Krasheninnikov, A.; Tolvanen, A.; Nordlund, K.; Keinonen, J. Effects of Ion Bombardment on a Two-dimensional Target: Atomistic Simulations of Graphene Irradiation. *Phys. Rev. B: Condens. Matter Mater. Phys.* **2010**, *81*, 153401.
(24) Koenig, S. P.; Wang, L.; Pellegrino, J.; Bunch, J. S. Selective Molecular Sieving Through Porous Graphene. *Nat. Nanotechnol.* **2012**, *7*, 728−732.
(25) Kim, H. W.; Yoon, H. W.; Yoon, S.-M.; Yoo, B. M.; Ahn, B. K.; Cho, Y. H.; Shin, H. J.; Yang, H.; Paik, U.; Kwon, S. Selective Gas Transport Through Few-Layered Graphene and Graphene Oxide Membranes. *Science* **2013**, *342*, 91−95.
(26) Jiang, D.-e.; Cooper, V. R.; Dai, S. Porous Graphene as the Ultimate Membrane for Gas Separation. *Nano Lett.* **2009**, *9*, 4019−4024.
(27) Du, H.; Li, J.; Zhang, J.; Su, G.; Li, X.; Zhao, Y. Separation of Hydrogen and Nitrogen Gases with Porous Graphene Membrane. *J. Phys. Chem. C* **2011**, *115*, 23261−23266.
(28) Hankel, M.; Jiao, Y.; Du, A.; Gray, S. K.; Smith, S. C. Asymmetrically Decorated, Doped Porous Graphene as an Effective Membrane for Hydrogen Isotope Separation. *J. Phys. Chem. C* **2012**, *116*, 6672−6676.
(29) Hauser, A. W.; Schwerdtfeger, P. Methane-Selective Nanoporous Graphene Membranes for Gas Purification. *Phys. Chem. Chem. Phys.* **2012**, *14*, 13292−13298.
(30) Drahushuk, L. W.; Strano, M. S. Mechanisms of Gas Permeation through Single Layer Graphene Membranes. *Langmuir* **2012**, *28*, 16671−16678.
(31) Qin, X.; Meng, Q.; Feng, Y.; Gao, Y. Graphene with Line Defect as a Membrane for Gas Separation: Design via a First-Principles Modeling. *Surf. Sci.* **2013**, *607*, 153−158.

(32) Liu, H.; Dai, S.; Jiang, D.-e. Permeance of H_2 through Porous Graphene from Molecular Dynamics. *Solid State Commun.* **2013**, *175*, 101−105.
(33) Zhang, H.; He, X.; Zhao, M.; Zhang, M.; Zhao, L.; Feng, X.; Luo, Y. Tunable Hydrogen Separation in sp-sp^2 Hybridized Carbon Membranes: A First-Principles Prediction. *J. Phys. Chem. C* **2012**, *116*, 16634−16638.
(34) Bieri, M.; Treier, M.; Cai, J.; Aït-Mansour, K.; Ruffieux, P.; Gröning, O.; Gröning, P.; Kastler, M.; Rieger, R.; Feng, X. Porous Graphenes: Two-Dimensional Polymer Synthesis with Atomic Precision. *Chem. Commun.* **2009**, *45*, 6919−6921.
(35) Blankenburg, S.; Bieri, M.; Fasel, R.; Müllen, K.; Pignedoli, C. A.; Passerone, D. Porous Graphene as an Atmospheric Nanofilter. *Small* **2010**, *6*, 2266−2271.
(36) Li, Y.; Zhou, Z.; Shen, P.; Chen, Z. Two-Dimensional Polyphenylene: Experimentally Available Porous Graphene as a Hydrogen Purification Membrane. *Chem. Commun.* **2010**, *46*, 3672−3674.
(37) Lu, R.; Rao, D.; Lu, Z.; Qian, J.; Li, F.; Wu, H.; Wang, Y.; Xiao, C.; Deng, K.; Kan, E. Prominently Improved Hydrogen Purification and Dispersive Metal Binding for Hydrogen Storage by Substitutional Doping in Porous Graphene. *J. Phys. Chem. C* **2012**, *116*, 21291−21296.
(38) Brockway, A. M.; Schrier, J. Noble Gas Separation using PG-ES X (X = 1, 2, 3) Nanoporous Two-Dimensional Polymers. *J. Phys. Chem. C* **2012**, *117*, 393−402.
(39) Schrier, J.; McClain, J. Thermally-Driven Isotope Separation across Nanoporous Graphene. *Chem. Phys. Lett.* **2012**, *521*, 118−124.
(40) Schrier, J. Fluorinated and Nanoporous Graphene Materials as Sorbents for Gas Separations. *ACS Appl. Mater. Interfaces* **2011**, *3*, 4451−4458.
(41) Jiao, Y.; Du, A.; Hankel, M.; Zhu, Z.; Rudolph, V.; Smith, S. C. Graphdiyne: A Versatile Nanomaterial for Electronics and Hydrogen Purification. *Chem. Commun.* **2011**, *47*, 11843−11845.
(42) Cranford, S. W.; Buehler, M. J. Selective Hydrogen Purification through Graphdiyne under Ambient Temperature and Pressure. *Nanoscale* **2012**, *4*, 4587−4593.
(43) Wall, Y.; Braun, G.; Kaltenborn, N.; Voigt, I.; Brunner, G. Separation of CO_2/N_2 by Means of a Carbon Membrane. *Chem. Eng. Technol.* **2012**, *35*, 508−512.
(44) Li, G.; Li, Y.; Liu, H.; Guo, Y.; Li, Y.; Zhu, D. Architecture of Graphdiyne Nanoscale Films. *Chem. Commun.* **2010**, *46*, 3256−3258.
(45) Chen, L.; Honsho, Y.; Seki, S.; Jiang, D. Light-Harvesting Conjugated Microporous Polymers: Rapid and Highly Efficient Flow of Light Energy with a Porous Polyphenylene Framework as Antenna. *J. Am. Chem. Soc.* **2010**, *132*, 6742−6748.
(46) Bieri, M.; Blankenburg, S.; Kivala, M.; Pignedoli, C. A.; Ruffieux, P.; Müllen, K.; Fasel, R. Surface-Supported 2D Heterotriangulene Polymers. *Chem. Commun.* **2011**, *47*, 10239−10241.
(47) Ourdjini, O.; Pawlak, R.; Abel, M.; Clair, S.; Chen, L.; Bergeon, N.; Sassi, M.; Oison, V.; Debierre, J.-M.; Coratger, R. Substrate-Mediated Ordering and Defect Analysis of a Surface Covalent Organic Framework. *Phys. Rev. B: Condens. Matter Mater. Phys.* **2011**, *84*, 125421.
(48) Marele, A. C.; Mas-Ballesté, R.; Terracciano, L.; Rodríguez-Fernández, J.; Berlanga, I.; Alexandre, S. S.; Otero, R.; Gallego, J. M.; Zamora, F.; Gómez-Rodríguez, J. M. Formation of a Surface Covalent Organic Framework Based on Polyester Condensation. *Chem. Commun.* **2012**, *48*, 6779−6781.
(49) Jackson, K. T.; Reich, T. E.; El-Kaderi, H. M. Targeted Synthesis of a Porous Borazine-linked Covalent Organic Framework. *Chem. Commun.* **2012**, *48*, 8823−8825.
(50) Schrier, J. Carbon Dioxide Separation with a Two-Dimensional Polymer Membrane. *ACS Appl. Mater. Interfaces* **2012**, *4*, 3745−3752.
(51) Zhang, T.; Xue, Q.; Shan, M.; Jiao, Z.; Zhou, X.; Ling, C.; Yan, Z. Adsorption and Catalytic Activation of O_2 Molecule on the Surface of Au-Doped Graphene under an External Electric Field. *J. Phys. Chem. C* **2012**, *116*, 19918−19924.
(52) Liu, Z.; Xue, Q.; Zhang, T.; Tao, Y.; Ling, C.; Shan, M. Carbon Doping of Hexagonal Boron Nitride by Using CO Molecules. *J. Phys. Chem. C* **2013**, *117*, 9332−9339.
(53) Grimme, S. Semiempirical GGA-Type Density Functional Constructed with a Long-Range Dispersion Correction. *J. Comput. Chem.* **2006**, *27*, 1787−1799.
(54) Sun, H. COMPASS: An ab Initio Force-field Optimized for Condensed-phase Applications Overview with Details on Alkane and Benzene Compounds. *J. Phys. Chem. B* **1998**, *102*, 7338−7364.
(55) Sun, H.; Ren, P.; Fried, J. The COMPASS Force Field: Parameterization and Validation for Phosphazenes. *Comput. Theor. Polym. Sci.* **1998**, *8*, 229−246.
(56) Rigby, D.; Sun, H.; Eichinger, B. Computer Simulations of Poly(ethylene oxide): Force Field, PVT Diagram and Cyclization Behaviour. *Polym. Int.* **1997**, *44*, 311−330.
(57) Shan, M.; Xue, Q.; Jing, N.; Ling, C.; Zhang, T.; Yan, Z.; Zheng, J. Influence of Chemical Functionalization on the CO_2/N_2 Separation Performance of Porous Graphene Membranes. *Nanoscale* **2012**, *4*, 5477−5482.
(58) Liu, Z.; Xue, Q.; Xing, W.; Du, Y.; Han, Z. Self-Assembly of C_4H-type Hydrogenated Graphene. *Nanoscale* **2013**, *5*, 11132−11138.
(59) Bieri, M.; Nguyen, M.-T.; Gröning, O.; Cai, J.; Treier, M.; Aït-Mansour, K.; Ruffieux, P.; Pignedoli, C. A.; Passerone, D.; Kastler, M. Two-Dimensional Polymer Formation on Surfaces: Insight into the Roles of Precursor Mobility and Reactivity. *J. Am. Chem. Soc.* **2010**, *132*, 16669−16676.
(60) Kumar, K. V.; Müller, E. A.; Rodríguez-Reinoso, F. Effect of Pore Morphology on the Adsorption of Methane/Hydrogen Mixtures on Carbon Micropores. *J. Phys. Chem. C* **2012**, *116*, 11820−11829.